aerospace

MDPI

Article

Research on the Trajectory Prediction of High-Altitude Zero-Pressure Balloon System Aiming to Rapidly Recover

Jiwei Tang[1], Shumin Pu[2,*], Peixi Yu [3], Weicheng Xie[4], Yunfei Li [5] and Binxing Hu[6]

[1] School of Aeronautics & Astronautics, Shanghai Jiao Tong University, Shanghai 200240, China, tangjw@sjtu.edu.cn
[2] Shanghai Jiao Tong University Chongqing Near Space Innovation R&D Center, Chongqing 401135, China; shuminpu@nsirdc.com
[3] Shanghai Jiao Tong University Chongqing Near Space Innovation R&D Center, Chongqing 401135, China; peixiyu@nsirdc.com
[4] Aerospace System Engineering Shanghai, Shanghai 200240, China; wei_cxie@126.com
[5] North Institute of Nuclear Technology, Xi'an 710000, China; lyf99961686@163.com
[6] Aerospace System Engineering Shanghai, Shanghai 200240, China; hubin8851@126.com

* Correspondence: shuminpu@nsirdc.com; Tel.: +86-18281029537

Abstract: A comprehensive simulation model is established to predict the trajectory of a high-altitude zero-pressure balloon flight system with no parachute equipped and only needs to carry the load floating at the designed altitude for several hours or less. A series of mathematical models, including thermal-dynamic, atmospheric, earth, wind, geometry, and exhaust models are developed to predict the trajectory of the balloon flight system. Based on these models, the uncertainties of the launch parameters and the corresponding flight performance are simulated. Combined with the control strategy, the entire flight trajectory including the ascending, floating and descending phases is simulated and discussed in detail. The results show that the vertical velocity takes on a "W" shape during the ascent process. What's more, the balloon begins to gradually descend with the solar radiation weakened after noon. Moreover, the landing vertical speed of the balloon flight system can approach to zero with the control strategy applied, while the lateral drift range is smaller relative to uncontrolled flight mode. The results and conclusions contribute to the design and operation of zero-pressure balloon flight system within limited airspace and improve the rapid recovery ability of the flight system.

Keywords: zero-pressure balloon; trajectory prediction; thermal-dynamic model; control strategy; rapid recovery

Citation: Lastname, F.; Lastname, F.; Lastname, F. Title. *Aerospace* **2022**, *9*, x. https://doi.org/10.3390/xxxxx

Academic Editor: Firstname Lastname

Received: date
Accepted: date
Published: date

Publisher's Note: MDPI stays neutral with regard to jurisdictional claims in published maps and institutional affiliations.

Copyright: © 2022 by the authors. Submitted for possible open access publication under the terms and conditions of the Creative Commons Attribution (CC BY) license (https://creativecommons.org/licenses/by/4.0/).

1. Introduction

With potential in civil and military applications including communication, observation and scientific research, there is a growing interest in studying platforms in near space [1-3]. The high-altitude zero-pressure balloon has become an indispensable test platform in near space because of its accessibility and affordability, which attracts the researchers from all over the world to conduct the corresponding research work [4-8].

In order to accomplish the mission of the balloon flight system, it's necessary to predict the balloon system's trajectory in advance, preventing the balloon that can float with the horizontal-direction wind from flying out of the required airspace. Throughout the flight mission, the uncertainties of the launch and environment parameters play an important role in predicting the flight performance, which has influence on the safe flight of the balloon. Failure of helium mass prediction will result in the balloon not reaching the designed altitude. Failure of helium temperature prediction will affect the trajectory

planning. Obviously, the effectiveness of trajectory prediction depends on the accuracy of the relevant parameters to optimize the balloon design and launch process.

In the recent years, many investigations have been carried out on high-altitude balloon trajectory predictions. Rodger E. Farley has designed a software program without considering the uncertainties during the flight process [9]. Qiumin Dai establishes a thermal-dynamic model of the super-pressure balloon, which emphasizes the importance of the film radiation property and clouds on balloon thermal behaviors [10]. András Sóbester develops a trajectory prediction model, which propose a new stochastic drag model based on empirical data derived from thousands of radiosonde flights to improve the prediction accuracy [11]. Yi Zhang takes the influences of the initial launch condition into consideration to simulate the balloon`s ascending process [12]. Yongseon Lee studies a trajectory prediction model which considers the uncertainties during the flight process [13]. Sherif Saleh develops an ascending performance prediction model, which optimizes the necessary inflating quantity of the helium to improve the ascending performance [14]. As we can see, the previous works mainly focus on the uncertainties about the thermal environment parameters and the launch parameters respectively, which have influences on the trajectory prediction`s accuracy.

Based on the previous work, this paper focuses on the trajectory prediction works of the high-altitude zero-pressure balloon within the limited airspace to optimize the balloon flight system rapid recovery. Firstly, a comprehensive simulation model is established to predict the flight performance and trajectory during the ascending, floating, and descending phases with various uncertainties considered. Secondly, taking the control strategies into consideration improves the balloon flight system fast recovery ability preventing the balloon from flying out the requested airspace to avoid possible accidents. All in all, since the balloon is unpowered which causes no way to control its horizontal motion, it`s necessary and significant to predict its trajectory after launching on the ground.

In this study, the balloon flight system descends without the separation between the balloon and the load, which contributes to reuse of the balloon capsule and the cost savings compared to exploding the balloon and relying on the parachute to recover the load. Fig. 1 shows the entire process of the flight mission of the balloon flight system, including the dynamic launching phase on the ground, the ascending phase, the floating phase and the descending phase.

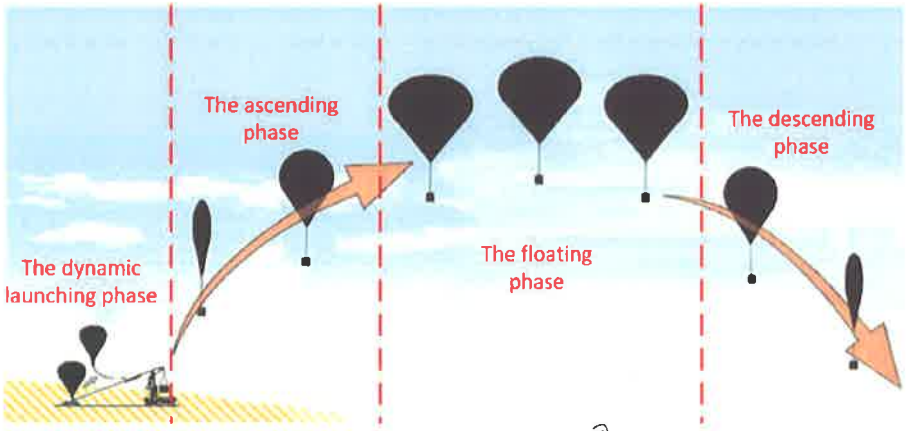


Figure 1. This figure shows the flight mission of balloon flight system.

2. Environment Model

During the flight process of the zero-pressure balloon, the differential temperature magnitude between the internal helium and the ambient atmosphere directly affects the net buoyancy of the balloon. Changes in environment parameters such as the surrounding atmosphere temperature, air pressure, air density, thermal radiation and acceleration of

the gravity during the flight process also directly or indirectly affect the internal helium temperature and the helium mass of the zero-pressure balloon. All of these variations should be taken into account to improve the accuracy of balloon system trajectory prediction.

2.1. Atmospheric Model

As altitude rises up, the atmospheric temperature, pressure and density vary with the altitude accordingly. In this study, the standard atmospheric model is used, which is released in 1976 [15]. The atmospheric temperature is defined as:

$$T_{air} = \begin{cases} 288.15 - 0.0065 * z & 0\ m < z \le 11000\ m \\ 216.65 & 11000\ m < z \le 20000\ m \\ 216.65 + 0.0010 * (z - 20000) & 20000\ m < z \le 32000\ m \end{cases} \quad (1)$$

The atmospheric pressure is defined as:

$$P_{air} = \begin{cases} 101325 * ((288.15 - 0.0065 * z)/288.15)^{5.25577} & 0\ m < z \le 11000\ m \\ 22632^{(-(z-11000)/6341.62)} & 11000\ m < z \le 20000\ m \\ 5474.87 * ((216.65 + 0.0010 * (z - 20000))/216.65)^{-34.163} & 20000\ m < z \le 32000\ m \end{cases} \quad (2)$$

According to the ideal gas law, the density is defined as:

$$\rho_{air} = P_{air}/(T_{air} * R_{air}) \quad (3)$$

Where z is the altitude, R_{air} refers to the gas constant of the air.

2.2. Thermal Model

Throughout the entire flight process of zero-pressure balloon, the balloon system is under the thermal environment. The researches [16] show that the main heat sources contain direct solar radiation, ground reflected radiation, sky scattered radiation, earth's infrared radiation, atmospheric infrared radiation, surface thermal radiation, convective heat transfer, and so on. Fig. 2 shows the heat sources for a high-altitude balloon system. And the direct solar radiation, the ground reflected radiation and the sky scattered radiation belong to the solar short-wave radiation. The earth's infrared radiation, the atmospheric infrared radiation and the surface thermal radiation belong to the long-wave radiation.

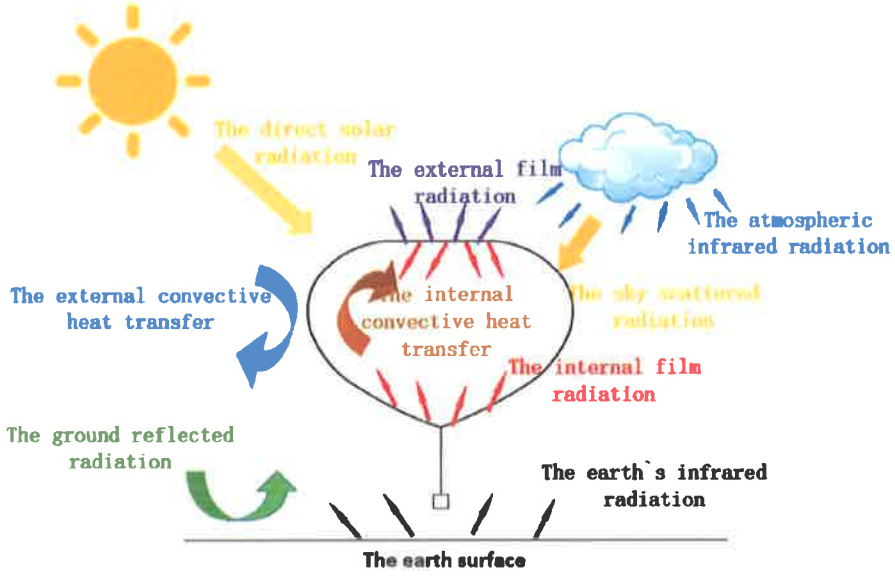


Figure 2. This figure shows heat sources for a high-altitude balloon system.

Through the heat transfer mechanism of thermal model, the heat is transferred among balloon film, internal helium and atmosphere [17]. Fig. 3 shows the heat transfer mechanism. The following contents illustrate the heat sources` models and the heat transfer relationships among atmosphere, balloon film and internal helium in detail.

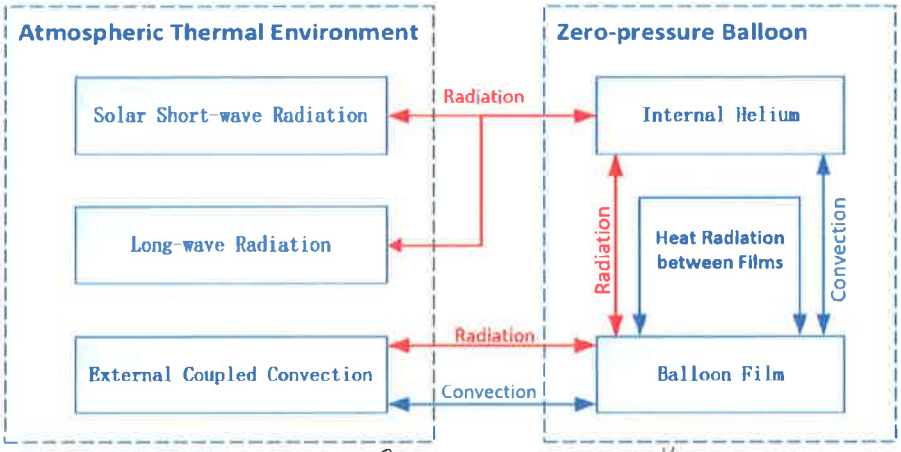


Figure 3. This figure shows heat transfer mechanism of thermal model.

2.2.1. Direct Solar Radiation

The absorption of direct solar radiation by balloon consists of the absorption by the outer surface and the absorption by the inner surface through balloon film, which is defined as follows:

$$Q_{Direct} = \alpha * A_{projected} * I_{sun} * \tau_{atm} * [1 + \tau * (1 + r_{effective})] \quad (4)$$

Where α indicates the film absorption factor of solar radiation, $A_{projected}$ indicates the illuminated projected area, I_{sun} indicates the solar radiation constant number, τ_{atm} is the atmospheric transmissivity factor of solar radiation, τ is the film transmissivity factor of solar radiation and $r_{effective}$ is the solar radiation effective reflectivity factor of balloon film.

The τ_{atm} is specified as:

$$\tau_{atm} = 0.5 * [e^{-0.65*Air_{Mass}} + e^{-0.95*Air_{Mass}}] \quad (5)$$

Where Air_{Mass} is the absolute atmospheric optical quality. As the altitude rises, the curvature`s radius of the earth changes, resulting in that the absolute atmospheric optical quality needs to be corrected in two forms [18]:

- Solar elevation angle $< 5°$:
  The Air_{Mass} is specified as:

$$Air_{Mass} = (\sin h + 0.457 * (90 - h)^{0.07}) * (6.484 + h)^{-1.697} * (\frac{P_{air}}{P_0})^{(0.488+0.15*h)} \quad (6)$$

- Solar elevation angle $> 5°$:
  The Air_{Mass} is specified as:

$$Air_{Mass} = (\sin h + 0.457 * (90 - h)^{0.07}) * ((6.484 + h)^{-1.697})^{-1} * \frac{P_{air}}{P_0} \quad (7)$$

Where h stands for the solar elevation angle, P_0 stands for the standard atmospheric pressure. And the solar elevation angle varies with the region, season, and the time of one day, which is formulated as:

$$\sin h = \sin \varphi * \sin \zeta + \cos \varphi * \cos \zeta * \cos \omega \quad (8)$$

Where φ refers to the local latitude, ζ refers to the solar declination angle, ω refers to the solar hour angle. The variation of the solar declination angle is the main cause of the variation of the solar radiation intensity on the earth`s surface, which is formulated as:

$$\zeta = 23.45 * \sin(2 * \pi * \frac{Nday + 284}{365}) \quad (9)$$

Where $Nday$ stands for the day serial number. The solar hour angle is defined as:

$$\omega = (TH - 12) * 15 \quad (10)$$

Where TH represents the true solar time. There are two reasons causing the time difference between true solar time and mean solar time: Firstly, the distance and relative position between the sun and the earth vary with time. Secondly, the earth`s equator doesn`t coincide with the plane of its orbit around the sun. The true solar time is specified as:

$$TH = TH_s \pm \frac{La - La_s}{15} + \frac{\Delta TH}{60} \quad (11)$$

Where TH_s stands for the regional standard time, La stands for the local longitude, La_s stands for the regional standard time position longitude, ΔTH stands for the time difference. The time difference is formulated as:

$$\Delta TH = -0.00167 + 7.36629 * \cos(W + 1.4981) - 9.92745 * \cos(2 * W - 1.26155) - 0.32123 * \cos(3 * W - 1.15710) \quad (12)$$

Where W represents the earth orbit time angle and is indicated by the following formula:

$$W = \frac{2 * \pi * Nday}{365} + 2 * e * \sin\left(\frac{2 * \pi * Nday}{365}\right) + 1.25 * e^2 * \sin(2 * \frac{2 * \pi * Nday}{365}) \quad (13)$$

Where e stands for the earth orbit eccentricity. And the $r_{effective}$ is formulated as:

$$r_{effective} = r + r^2 + r^3 + r^4 + r^5 + \cdots \quad (14)$$

2.2.2. Ground Reflected Radiation

The ground reflected radiation is specified as:

$$Q_{Albedo} = \alpha * \rho_{earth} * A_{surf} * I_{sun} * \sin h * \tau_{ViewFactor} * [1 + \tau * (1 + r_{effective})] \quad (15)$$

Where ρ_{earth} indicates the earth surface reflectance factor, $\tau_{ViewFactor}$ indicates the angular coefficient from balloon surface to earth surface, A_{surf} stands for the Surface area of the zero-pressure balloon.

2.2.3. Sky Scattered Radiation

The sky scattered radiation is formulated as:

$$Q_{Scatter} = 0.5 * \alpha * A_{surf} * I_{sun} * \sin h * \tau_{ViewFactor} * \frac{Air_{Mass} * (1 - \tau_{atm})}{Air_{Mass} - 1.4 * \ln \tau_{atm}} * [1 + \tau * (1 + r_{effective})] \quad (16)$$

2.2.4. Earth`s Infrared Radiation

The earth`s infrared radiation is indicated by the following formula:

$$Q_{IR,earth} = \alpha_{IR} * \varepsilon_{earth} * \sigma * T_{earth}^4 * A_{surf} * \tau_{ViewFactor} * \tau_{atm,IR} * [1 + \tau_{IR} * (1 + r_{effective,IR})] \quad (17)$$

Where α_{IR} represents the film absorption factor of infrared radiation, ε_{eart} represents the ground average infrared emissivity factor, σ represents the Stefan-Boltzmann constant, τ_{IR} represents the film transmissivity factor of infrared radiation, $r_{effective,IR}$ represents the infrared radiation effective reflectivity factor of balloon film, T_{eart} represents the earth surface temperature, And the $\tau_{atm,IR}$ represents the atmospheric transmissivity factor of the infrared radiation.

2.2.5. Atmospheric Infrared Radiation

The atmospheric infrared radiation is formulated as:

$$Q_{IR,Sky} = \alpha_{IR} * \sigma * \varepsilon_{sky} * T_{sky}^4 * A_{surf} * (1 - \tau_{ViewFactor}) * [1 + \tau_{IR} * (1 + r_{effective,IR})] \quad (18)$$

Where ε_{sky} stands for the atmospheric average infrared emissivity factor. And the T_{sky} stands for the sky equivalent temperature, which is defined as:

$$T_{sky} = 0.052 * T_{air}^{1.5} \quad (19)$$

2.2.6. Surface Thermal Radiation

The infrared radiation of the film includes the film external surface and the film internal surfaces` infrared radiation. The total surface thermal radiation is calculated by the following formula [19]:

$$Q_{IR,film} = Q_{IR,out} - Q_{IR,absorb} = \varepsilon * \sigma * 2 * A_{surf} * T_{film}^4 - \sigma * \varepsilon * \alpha_{IR} * A_{surf} * T_{film}^4 * (1 + r_{effectivce,IR}) \quad (20)$$

Where the ε stands for the average infrared emissivity factor of film material, the T_{film} stands for the temperature of the film.

2.2.7. Convective Heat Transfer

The convective heat transfer of high-altitude balloon includes the convective heat transfer between the film and the external atmosphere and the convective heat transfer between the film and the internal helium.

For the convective heat transfer between the film and the external atmosphere, there are two types of convective modes called natural convection and forced convection, which are defined as:

$$Q_{ConvExt} = H_{external} * A_{surf} * (T_{air} - T_{film}) \quad (21)$$

Where $H_{external}$ represents the external convection heat transfer coefficient. For the convection heat transfer between the film and the external atmosphere, it`s usually a coupled heat transfer process, so the $H_{external}$ is specified as:

$$H_{external} = (H_{force}^3 + H_{free}^3)^{1/3} \quad (22)$$

Where H_{force} represents the forced convection heat transfer coefficient, H_{free} represents the natural convection heat transfer coefficient.

For the convection heat transfer between the film and the internal helium, its convective mode is the natural convection, which is specified as:

$$Q_{ConvInt} = H_{internal} * A_{surf} * (T_{film} - T_{helium}) \quad (23)$$

Where the T_{hel} is the temperature of the helium.

2.2.8. Heat Transfer on Balloon Film

In this study, the temperature of the film is assumed to be uniform which is formulated as [9]:

$$\frac{dT_{film}}{dt} = \frac{Q_{sun} + Q_{Albedo} + Q_{scatter} + Q_{IR,earth} + Q_{IR,sky} + Q_{ConvExt} - Q_{ConvInt} - Q_{IR,film}}{C_f * m_{film}} \quad (24)$$

Where the C_f is the specific heat capacity of the film material, Q_{sun} stands for direct solar radiation, Q_{Albedo} stands for ground reflected radiation, $Q_{scatter}$ stands for sky scattered radiation, $Q_{IR,earth}$ stands for earth`s infrared radiation, $Q_{IR,sky}$ stands for atmospheric infrared radiation, $Q_{ConvExt}$ and $Q_{ConvInt}$ stands for convective heat transfer, $Q_{IR,film}$ stands for surface thermal radiation.

2.2.9. Heat Transfer on Internal Helium

This study also assumes that temperature and pressure of the internal helium are uniform. According to the first law of thermodynamics, the temperature change rate of the internal helium is specified as [9]:

$$\frac{dT_{helium}}{dt} = \frac{Q_{ConvInt}}{C_v * m_{helium}} + (\gamma - 1) * T_{helium} * \left(\frac{dm_{helium}}{dt} * \frac{1}{m_{helium}} - \frac{dVolume_{helium}}{dt} * \frac{1}{Volume_{helium}}\right) \quad (25)$$

Where C_v represents the specific heat capacity at constant volume of helium. The γ represents the specific heat ratio, which equals to the C_p/C_v. And C_p represents the specific heat capacity at constant pressure of helium.

2.3. Earth Model

As the balloon flight system moves on, the local earth radius and gravity change with the location. In this study, the WGS-84 earth model is used to offer the real-time data of the earth radius and the acceleration of the gravity at the current balloon location. The corresponding equations are defined as [20]:

$$R_{meridian} = \frac{r_e * (1 - \varepsilon^2)}{(1 - \varepsilon^2 * (\sin\varphi)^2)^{3/2}} \quad (26)$$

$$R_{normal} = \frac{r_e}{(1 - \varepsilon^2 * (sin\,\varphi)^2)^{1/2}} \quad (27)$$

$$R_{equiv} = \sqrt{R_{meridian} * R_{normal}} \quad (28)$$

$$g = g_{WGS_0} \frac{1 + g_{WGS_1} * (\sin\varphi)^2}{(1 - \varepsilon^2 * (sin\,\varphi)^2)^{1/2}} \quad (29)$$

Where $R_{meridian}$ stands for meridian radius, R_{normal} stands for normal radius, R_{equiv} stands for equivalent radius, g stands for acceleration of the gravity, r_e stands for equatorial radius, ε stands for first eccentricity, g_{WGS_0} stands for gravity acceleration at equator, g_{WGS_1} stands for gravity formula constant.

3. Trajectory Prediction Model

In order to simulate the motion of the balloon, some hypotheses are regulated:

(1) The horizontal components of the balloon`s speed and its speed relative to that of atmosphere winds are considered to be small;

(2) The balloon is assumed to be a point mass when considering the external forces acting on the balloon;

(3) The high-altitude wind speed`s magnitude and direction are assumed to be the same within 24 hours.

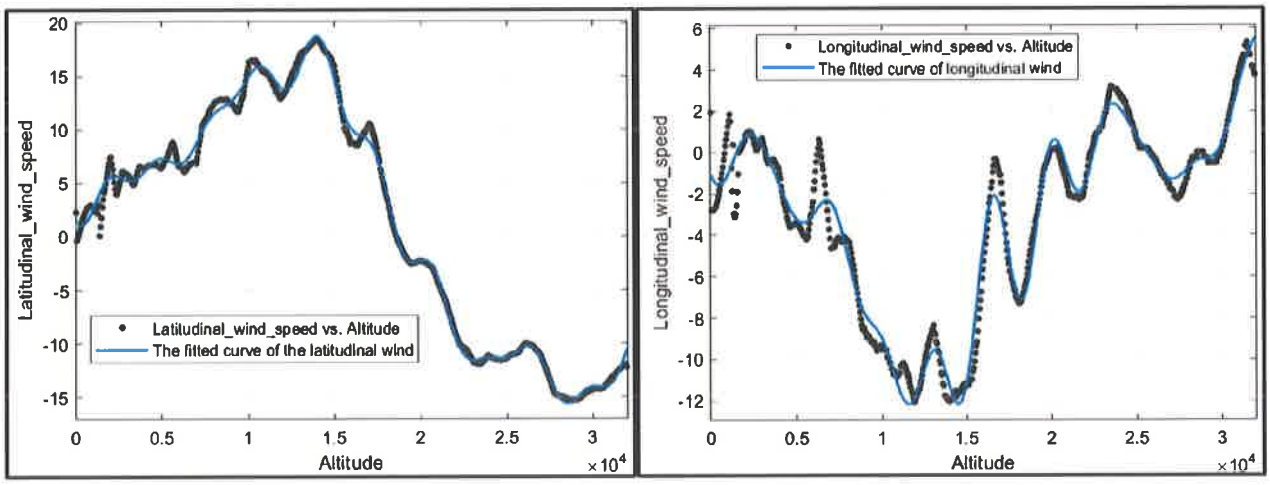
3.1. Wind Model

As the altitude rises up, the wind speed`s magnitude and direction change with the altitude. And the wind direction is usually divided into latitudinal wind and longitudinal wind. For latitudinal wind, the western wind is positive, while for longitudinal wind, the southern wind is positive.

In this study, the wind data are measured on 8 August, 2019 (UTC+16) in China, which contain the wind speed magnitude and direction from the ground to the 32km altitude. After the data processing, these discrete wind data are fitted to a series of continuous curves by the Sum of Sines Models, which is specified as [21]:

$$y = \sum_{i=1}^{n} a_i * \sin(b_i * x + c_i) \quad (30)$$

Where a represents amplitude, b represents frequency, and c represents phase constant for each sine wave term. The n is the number of terms in the series and $1 \le n \le 8$. Fig. 4 shows the discrete wind data and the corresponding fitted curve.



(a) (b)

Figure 4. This figure shows the discrete wind data and the corresponding fitted curve. (a) shows the discrete latitudinal wind data and the fitted curve of the latitudinal wind; (b) shows the discrete longitudinal wind data and the fitted curve of the longitudinal wind.

graphs are missing units on both axes

these

Based on the above fitting results, the corresponding fitted curves are defined as:

(1) The fitted curve of the latitudinal wind speed(m/s) vs. altitude(m):

add space

$$f(x)_{latitude} = \sum_{i=1}^{8} a_i * \sin(b_i * x + c_i) \quad (31)$$

uncap.

Where x indicates altitude and $f(x)_{latitude}$ is the latitudinal wind speed at the corresponding altitude, $a_i = [23.39, 30.97, 7.256, 35.02, 1.212, 1.159, 34.26, 0.9401]$, $b_i = [7.183e-05, 3.544e-05, 0.00031, 0.00099, 0.001989, 0.000675, 0.000992, 0.00165]$, $c_i = [0.4929, 3.151, 3.723, 5.658, -1.421, -2.213, 2.584, -2.243]$.

(2) The fitted curve of the longitudinal wind speed(m/s) vs. altitude(m):

add space

$$f(x)_{longitude} = \sum_{i=1}^{8} a_i * \sin(b_i * x + c_i) \quad (32)$$

uncap.

Where x indicates altitude, the $f(x)_{longitude}$ is the longitudinal wind speed at the corresponding altitude, $a_i = [80.21, 3.932, 80.58, 1.416, 1.007, 0.2995, 0.8878, 1.157]$, $b_i = [8.839e-05, 0.00036, 9.238e-05, 0.0018, 0.00078, 0.00123, 0.0029, 0.001476]$, $c_i = [-0.7307, 0.3148, 2.454, -2.866, 1.572, -0.4936, -1.095, 2.805]$.

3.2. Geometry Model

a

The zero-pressure balloon with shape factor of 0.2 is employed as the research subject. The detailed geometric equations are as follows [9]:

object

Usually "subject" (of research) is a living thing

(1) Diameter from the top view:

$$Diameter = 1.383 * Volume^{1/3} \quad (33)$$

(2) Projected area from the top view:

$$A_{top} = \frac{\pi}{4} * Diameter^2 \quad (34)$$

(3) During the balloon flight process, the illuminated projected area varies with the solar elevation angle, which is defined as:

$$A_{projected} = A_{top} * [0.9125 + 0.0875 * \cos(\pi - 2 * h)] \quad (35)$$

(4) Surface area of the zero-pressure balloon:

$$A_{surf} \approx 4.94 * Volume^{2/3} \quad (36)$$

(5) When the balloon isn't fully inflated, the surface of the balloon is presented in "crenellated" form. The maximum crenellated surface area is defined as follows:

$$A_{surf1} = 4.94 * Volume_{design}^{2/3} * (1 - \cos(\pi * L_{goreB}/L_{goreDesign})) \quad (37)$$

Where L_{goreB} indicates length of gore exposed in the balloon, $L_{goreDesign}$ indicates designed gore of the balloon, $Volume_{design}$ indicates the maximum volume of the balloon.

(6) To better approximate the realistic situation for convection and film mass calculations, $A_{effective}$ is used to describe the effective exposed surface area:

$$A_{effective} = 0.65 * A_{surf} + 0.35 * A_{surf1} \quad (38)$$

(6) The zero-pressure balloon has a distinctive feature that the internal helium pressure almost equals to the surrounding atmosphere pressure. Therefore, based on the ideal gas law, the balloon's volume can be formulated as:

$$Volume = \frac{m_{helium} * R_{helium} * T_{helium}}{P_{helium}} \quad (39)$$

$$P_{helium} = P_{air} \quad (40)$$

Where $Volume$=$Volume_{balloon}$=$Volume_{helium}$, R_{helium} stands for helium gas constant, T_{helium} stands for helium temperature, P_{helium} stands for helium pressure and P_{air} stands for surrounding atmosphere pressure.

3.3. Dynamic Model

The motion of the zero-pressure balloon is divided into the vertical motion and the horizontal motion. For the vertical motion, the gross external force contains buoyant force, gross weight and aerodynamic drag force. The vertical dynamic equation of motion is defined as [22]:

$$m_{virtual} * \frac{dv_z}{dt} = (\rho_{air} - \rho_{helium}) * Volum * g - m_{gross} * g - \frac{1}{2} * C_d * \rho_{air} * A_{top} * v_z^2 \quad (41)$$

Where v_z is the vertical speed of the balloon flight system, m_{gross} is the gross mass of payload, film and ballast, $m_{virtual}$ is the gross mass of payload mass, film mass, ballast mass, helium mass and air virtual mass. And air virtual mass is specified as:

$$m_{air,virtual} = C_{vir} * \rho_{air} * Volume_{helium} \quad (42)$$

Where C_{vir} stands for virtual mass coefficient, and $C_{vir} \approx 0.5$. C_d stands for drag coefficient, which is defined as [23]:

$$\begin{cases} C_d = 1.5 * (\frac{24}{Re} + \frac{6}{1+\sqrt{Re}} + 0.4), & Re \le 2.7 * 10^5 \\ \log C_d = 1.5 * (25.821 - 4.825 * \log Re), & 2.7 * 10^5 < Re \le 3.7 * 10^5 \\ \log C_d = 1.5 * (-0.699 - 0.347 * e^{-3.533*(\log\frac{Re}{3.7*10^5})^{5.306}}), & 3.7 * 10^5 < Re \le 10^6 \\ C_d = 0.3, & Re > 10^6 \end{cases} \quad (43)$$

For the horizontal motion, the balloon is regarded as floating with the wind, assuming that the horizontal velocity is equal to the wind speed magnitude. The horizontal dynamic equation is defined as:

$$v_{east} = \frac{dx_{latitude}}{dt} = v_{wind} * \sin\theta \quad (44)$$

$$v_{north} = \frac{dx_{longitude}}{dt} = v_{wind} * cos\,\theta \quad (45)$$

Where v_{east} and v_{nort} are the longitudinal and latitudinal balloon speed, respectively, $x_{latitude}$ and $x_{longitude}$ are the longitudinal and latitudinal distance, respectively. The θ indicates the angle between the direction of horizontal wind and the due north of earth. In the earth coordinate system, the balloon`s horizontal displacements are defined as [24]:

$$\dot{Lat} = \frac{v_{north}}{R_{meridian} + ALT} \quad (46)$$

$$\dot{Lon} = \frac{v_{east}}{(R_{normal} + ALT) * \cos Lat} \quad (47)$$

Where ALT indicates altitude. Lat and Lon indicate latitude and longitude respectively.

3.4. Exhaust Model

3.4.1. Automatic exhaust model

The zero-pressure balloon`s ascending process contains two phases, one with balloon partially expanded and the other with balloon fully expanded.

The balloon is fully expanded means that the balloon has expanded to its designed volume, then the overfilled helium is automatically vented from the exhaust pipes which is installed at the bottom of the balloon, preventing the balloon from explosion. This helium exhaust process is called automatic exhaust process. The corresponding helium mass loss is defined as:

$$\frac{dm_{helium}}{dt} = -\rho_{helium} * \frac{Volume_{altitude} - Volume_{design}}{dt} \quad (48)$$

Where ρ_{helium} stands for density of the helium, $Volume_{altitude}$ stands for balloon volume with corresponding altitude. The equation works on the premise that the balloon has expanded to its designed volume.

3.4.2. Active exhaust model

Considering the realistic flight mission requirements and some emergencies, the balloon flight system needs to be forced to descend. At this moment, the helium exhaust valve installed at the apex of the balloon will be immediately opened to exhaust the helium. This helium exhaust process is called "active" exhaust process. The corresponding helium mass loss is specified as [25]:

$$\frac{dm_{heli}}{dt} = -\rho_{helium} * c * A * \sqrt{\frac{2 * \Delta P}{\rho_{helium}}} \quad (49)$$

Where c indicates helium flow coefficient depending on the number and the shape of the helium exhaust valve, and A indicates the total opening area of the exhaust valve.

3.5. Ballast Model

As daylight hours pass, the intensity of solar radiation gradually weakens, causing the internal helium temperature to drop as well, and the volume of the balloon starts to shrink sequentially. Finally, the zero-pressure balloon flight system begins to descend. In order to keep the designed altitude stable or to control the vertical landing velocity, a corresponding mass of ballast needs to be threw.

In this study, the granular iron sand is used as ballast, and the ballast discharge rate is determined experimentally by a throwing ballast device before the balloon flight mission. The ballast model is defined as:

$$m_{ballast_{remained}} = m_{ballast_{actual}} - \int_0^t k_{ballast}\,dt \quad (50)$$

Where $m_{ballast_{actual}}$ stands for the mass of ballast before throwing, $m_{ballast_{remained}}$ stands for the mass of ballast after throwing, $k_{ballast}$ stands for ballast flow rate.

4. Results and Discussion

The simulation program is done by the Matlab/Simulink and the corresponding simulation program structure diagram is showed in Fig. 5. Fig. 5 shows the above models including atmospheric model, thermal model, earth model, wind model, geometry and exhausted model, dynamic model, ballast model, and so on. The simulation process is realized through the data flow among models and the above nonlinear differential equations are solved by Runge-Kutta methods.

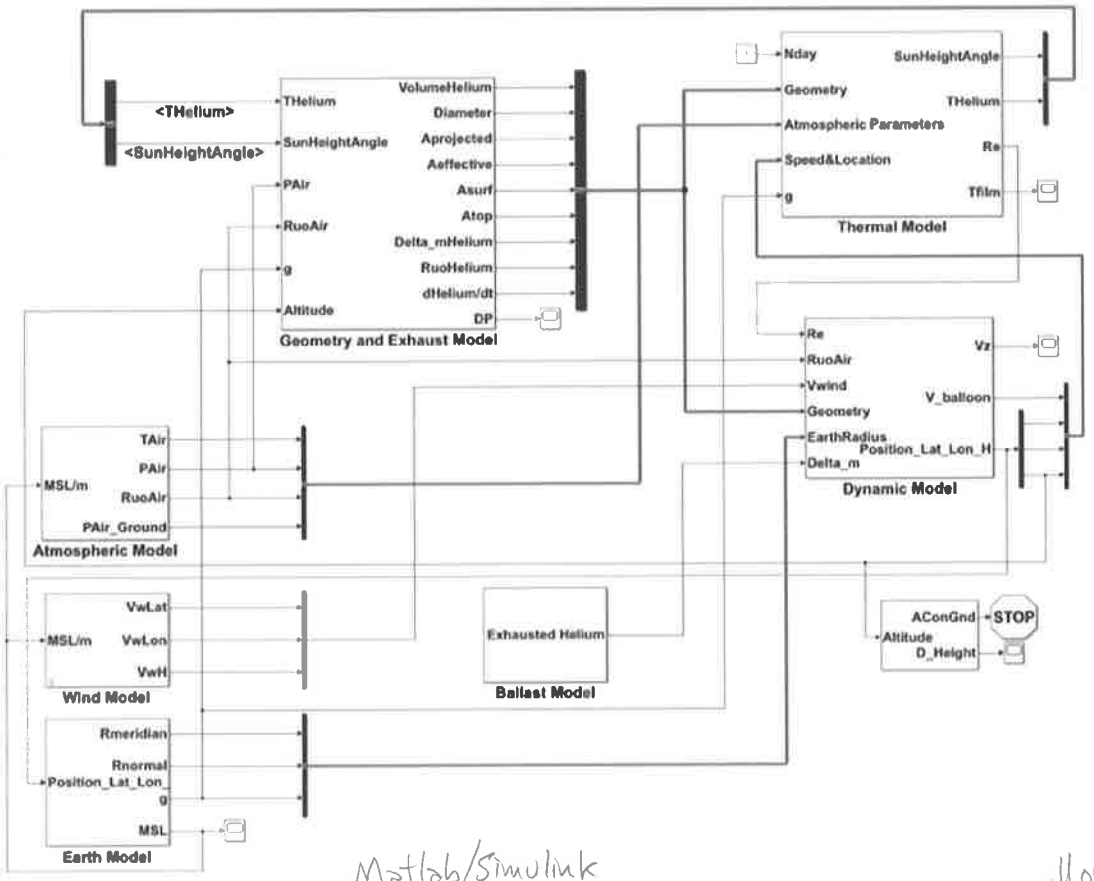


Figure 5. This figure shows the simulation program structure diagram.

4.1. Model Validation

The best way to verdict the simulation program would be to compare the simulation results with the real flight recorded data. However, the flight mission data, balloon specification, atmospheric information and film surface characteristics can't be easily got. In this paper, the NASA's Scientific Balloon Analysis Model (SINBAD) and Palumbo et al.'s Analysis Model for High-Altitude Balloon (ACHAB) are used to validate the present model [26-27]. Both models have been proved to offer highly accurate trajectory prediction, which are compared with the real flight data [13,27]. And the corresponding input data and output data can be found in this work [27]. Based on the previous work, the drag

coefficient is taken into consideration for model validation. The varying drag coefficient is used for ACHAB and present models, which is defined by corresponding functions. And the constant drag coefficient of 0.45 is used for ACHAB, SINBAD and present model, respectively. The simulation results are shown in Fig. 6.

On the left side of Fig. 6, the vertical velocity profile of the present model seems to be similar to that of ACHAB and the SINBAD models with the constant drag coefficient. The reason for difference at the initial time and the time of reaching the designed altitude is that the ground surface temperature model and atmospheric model are different, which affects the ascent flight performance. For the varying coefficient, the time of reaching the designed altitude for both models is the same. Apparently, all of the velocity profile takes on a W shape. On the right side of Fig. 6, the present model is slightly lower than the previous program. The reason for this is that atmosphere density and gravity acceleration differences mainly affect the net buoyancy at the designed altitude. In the present model, the variation of gravity with position is considered, while for the other models it's not considered.

In summary, the present model appears to be similar to the previous simulation programs and can offer enough accuracy for trajectory prediction. However, it still needs to optimize the simulation program with an interpolation model that considers the relationship of height and drag coefficient, since the balloon geometry changes with altitude during the ascent phase.

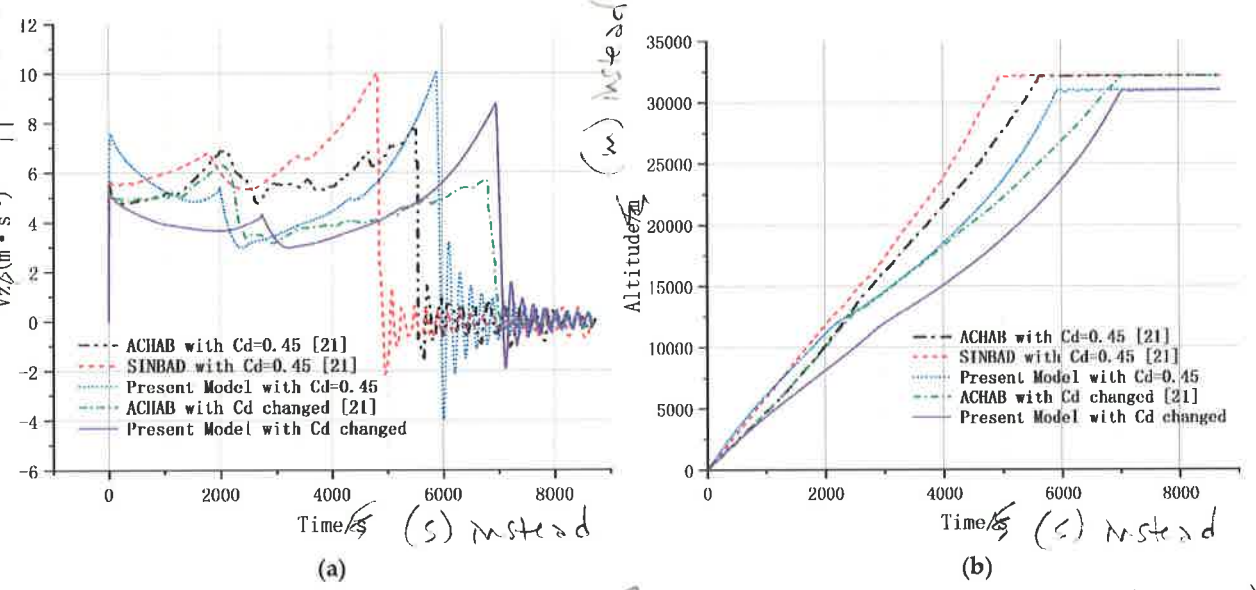


Figure 6. This figure shows the simulation results. (a) shows the comparison of the vertical speed; (b) shows the comparison of the altitude.

4.2. Flight Simulation

The zero-pressure balloon's specifications and the corresponding flight simulation information are presented in Table 1. The flight performance is simulated during the entire trajectory in detail.

Table 1. Balloon's specifications and flight simulation information.

Parameter	Value
Maxi volume	44930.5m³
Lifting gas(helium) mass	626.5kg
Balloon mass	487kg

Suspending mass(payload)	2930.87kg
Initial film temperature	286.95K
Initial helium temperature	286.95K
Number of the helium exhaust valve	2
Film absorption factor of solar radiation	0.33
Film transmissivity factor of solar radiation	0.65
Film absorption factor of infrared radiation	0.75
Film transmissivity factor of infrared radiation	0.20
Film average infrared emissivity factor	0.75
Earth surface reflectance factor	0.3
Ground average infrared emissivity factor	0.95
Launch time	On 8 August, 2019 (UTC +16)
Launch base	Lat:39°, lon:105°
Target altitude	20km
Ground air pressure	101325pa
Ground air temperature	288.15K

The variation of film temperature, internal helium temperature, atmospheric temperature, altitude, exhausted helium mass, vertical velocity and trajectory throughout the flight mission are shown in Fig. 7, Fig. 8, Fig. 9 and Fig. 10.

1. The change pattern of temperature

During the ascending phase, the temperature of film and helium decreases simultaneously with the atmospheric temperature in the way of same tendency. In addition, the temperature of both film and helium are lower than atmospheric temperature, causing the phenomenon of supercooling. And the maximum temperature difference reaches -17.2 ℃ between helium and surrounding atmosphere. The reason for this is that the volume of the balloon expands rapidly and the internal helium dose positive work on the external atmosphere.

After the balloon flight system reaches the designed altitude, the temperature of film and helium gradually increases and comes to an equilibrium with the ambient thermal environment. The trend of temperature increase becomes stable and the increase tends to be approximately equal. After sunrise, the internal helium and film temperatures rise rapidly again due to solar radiation, with the temperature difference reaching a peak at noon. The corresponding temperature difference between the helium and the surrounding atmosphere is +54.55°C.

In the afternoon, the temperature of the internal helium begins to drop as the solar radiation decreases, resulting in a decrease in balloon volume and net buoyancy. The balloon begins to move downward. During the descent, the external atmosphere does work on the helium expansion and the solar radiation still does work, effectively compensating the surface of the balloon so that helium temperature changes very little in the stratospheric range. After entering the tropospheric range, the temperature of the helium rises rapidly, causing the phenomenon of superheating. And by the time it reaches the ground, the helium temperature can reach 43°C eventually.

2. The change pattern of altitude

The ascent and descent processes of the balloon flight system are manipulated by the vertical velocity. As shown in Fig. 9 and Fig. 11, the ascent time of the balloon flight system is almost 75 minutes faster than the descent process. In addition, during the floating phase, the balloon reaches its designed volume. The increase in helium temperature causes the internal helium to expand and the corresponding amount of

helium is continuously discharged from the bottom exhaust pipe, causing the balloon flight system to move upward due to the buoyancy force being greater than gravity. The maximum altitude eventually reached 20,200.9 meters. After reaching the maximum altitude, the balloon flight system starts to move downward.

3. The change pattern of vertical speed

Throughout the ascent process, the vertical velocity changes in a "W" pattern. Initially, the balloon flight system rises rapidly and its vertical velocity increases sharply to 9.285 m/s. Then the vertical velocity decreases due to the weakening of the upward net buoyancy caused by the supercooling properties of the internal helium. After reaching a certain altitude, the atmospheric density reduces to a minimum magnitude, resulting in the drag goes down to a relatively small value and the vertical speed to increase.

Moreover, when the balloon flight system climbs above 11 km, the vertical velocity decreases significantly and then increase again. Furthermore, when the balloon flight system is about to reach the designed altitude, the vertical velocity drops sharply and oscillates around 0 until it finally drops gradually to 0. In the afternoon, influenced by the surrounding thermal environment, the balloon flight system starts to descend and its downward vertical velocity continues to increase, reaching 8.331 m/s by the time it lands on the ground.

4. The change pattern of the total exhausted mass of helium

The high-altitude zero-pressure balloon has a unique and distinctive feature that there are exhausted pipes installed at the bottom of the balloon for exhausting the excessive helium. This is the reason why the zero-pressure balloon flight system can't float for a long time, so it is imperative to figure out the helium exhausted process in detail to plan the flight mission.

From the results described in Fig. 7 and Fig. 9, it is illustrated that the ascent process can be divided into two phases, including non-forming and forming geometry phases. The non-forming geometry phase occurs mainly at the initial time of the ascent process. As the external atmospheric pressure decrease, the volume of the balloon keeps expanding and the helium mass remains constant. When the balloon flight system is about to reach the design altitude, the forming geometry phase appears. In this phase, the volume of the balloon reaches its maximum and remains unchanged. Due to the momentum and vertical velocity, the balloon flight system continues to rise, causing excess helium to be discharged from the corresponding tubes. The helium mass begins to be lost.

During the floating phase, the loss of helium mass continues which is proportional to the solar radiation. After the balloon flight system begins to descend, the balloon begins to shrink, but the helium mass keeps constant gain until it reaches the ground. During the entire flight process, the total exhausted mass of helium is ~~almost~~ ~~up to~~ 183.1 kg.

5. Trajectory prediction

As shown in Fig. 10, the straight-line distance between the launch base and the landing site is 435.723 km, and the azimuth between the launch base site and the landing site point is 266.9°. Moreover, the flight mission lasts for nearly 18 hours. Apparently, the high-altitude zero-pressure balloon flies in a huge airspace without corresponding control strategy and the trajectory takes on a "Z" shape.

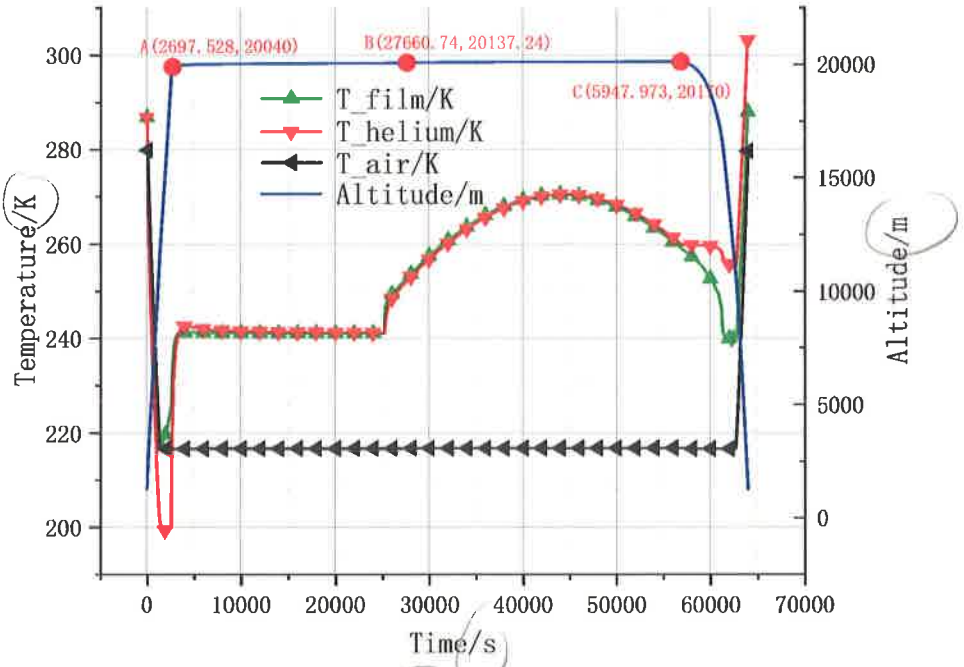


Figure 7. ~~This figure shows~~ the temperature change of film, helium and air vs. time and the altitude change vs. time.

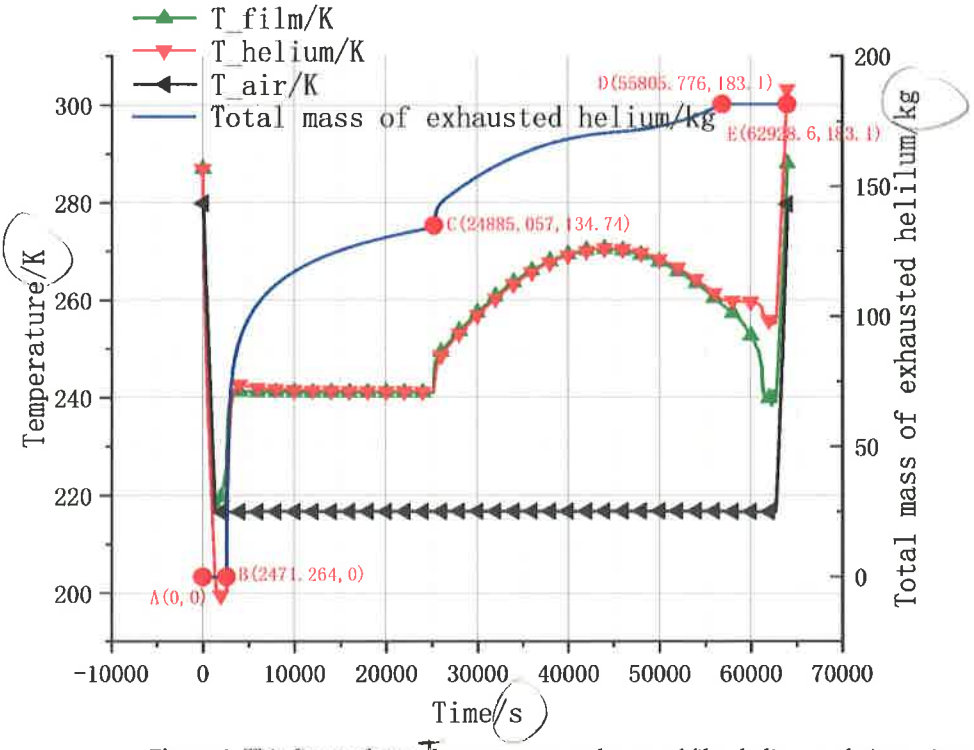


Figure 8. ~~This figure shows~~ the temperature change of film, helium and air vs. time and change of the total mass of exhausted helium vs. time.

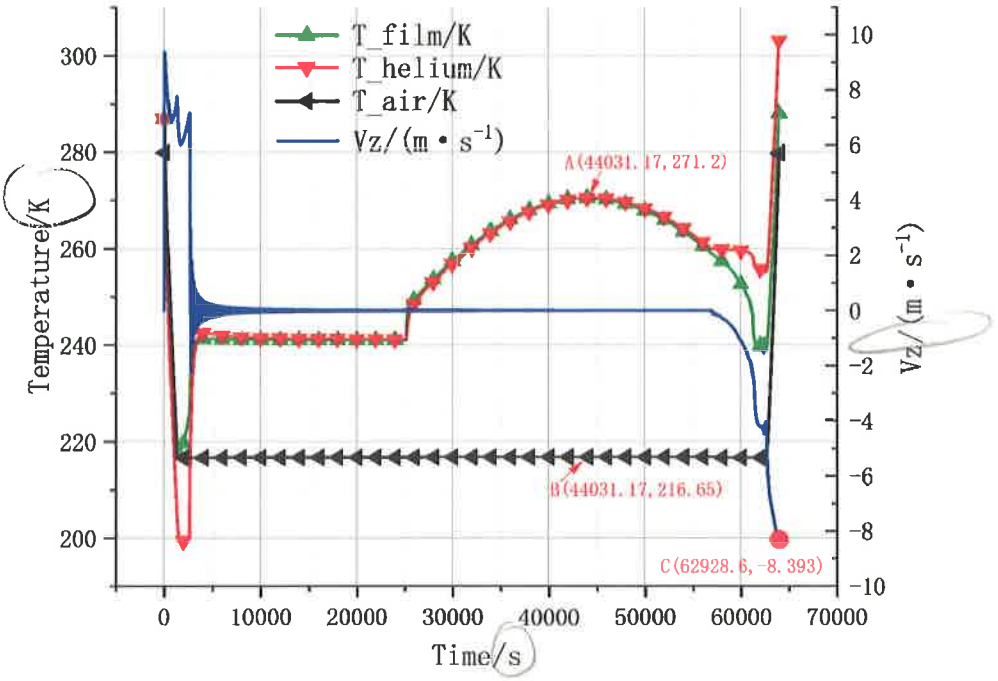


Figure 9. ~~This figure shows~~ the temperature change of film, helium and air vs. time and change of the vertical speed of the balloon flight system vs. time.



(a) **(b)**

Figure 10. ~~This figure shows~~ the trajectory of the balloon flight system. (**a**) shows the relative position of trajectory in the world map; (**b**) shows the trajectory in detail.

Based on ~~the~~ above results, the balloon performance is discussed in detail during the entire flight mission, which helps for the balloon system design and operation. What's more, it can be concluded that the vertical speed during landing has a serious impact on the safe recovery of the balloon flight system. In addition, the flight time and flight distance are not conducive to the rapid recovery of the balloon flight system. It is imperative to clarify the impact of the uncertainty of the launch parameters on the trajectory prediction and to develop corresponding control strategy to improve the rapid recovery and achieve efficient and safe application of high-altitude zero-pressure balloon flight system in limited airspace.

4.2.1. The Launch Time

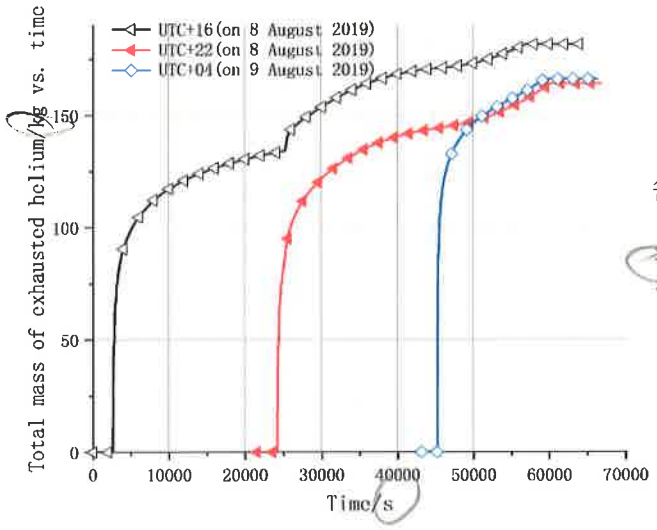
The different launch times including UTC 16 on 8 August, UTC 22 on 8 August and UTC 04 on 9 August are used to simulate the flight mission. As shown in Fig. 11, the launch time plays an important role in the trajectory prediction. ~~The reason for this is that~~

direct solar radiation, ground reflected radiation, sky scattered radiation and other thermal radiation have a periodical change characteristic with time, causing a great difference of radiation at different moments.

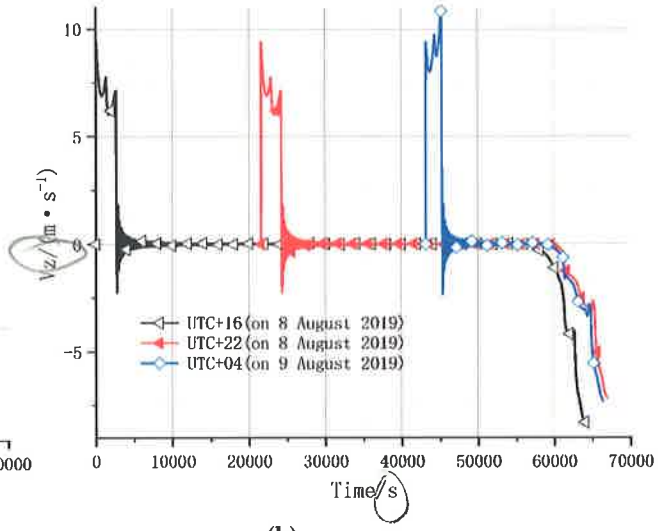
By comparing the flight performance of zero-pressure balloon system at different time, it is concluded that:

1. The earlier the launch time, the more total mass of helium is exhausted finally.
2. The earlier the launch time, the smaller vertical velocity during the accent phase and the relatively low requirements for balloon structure design.
3. The launch time almost has no effect on the floating altitude and the landing vertical velocity.
4. The earlier the launch time, the longer the flight time and the flight distance. However, the maximum flight time is less than 24 hours.

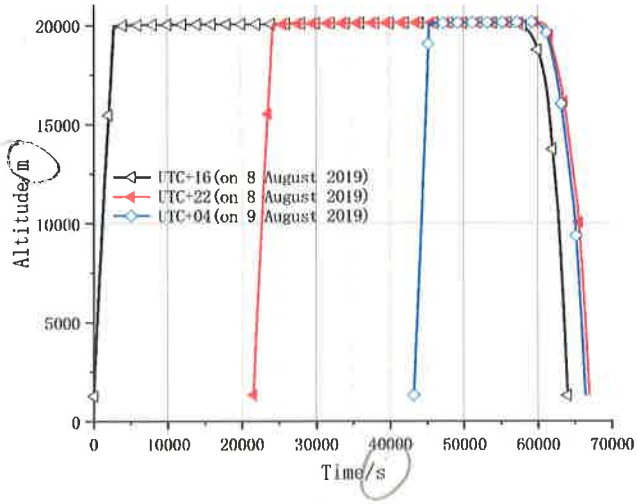
According to the above results, it's rightful to choose the suitable launch time to start the flight mission and meet the mission requirements.



(a)



(b)



(c)



(d)

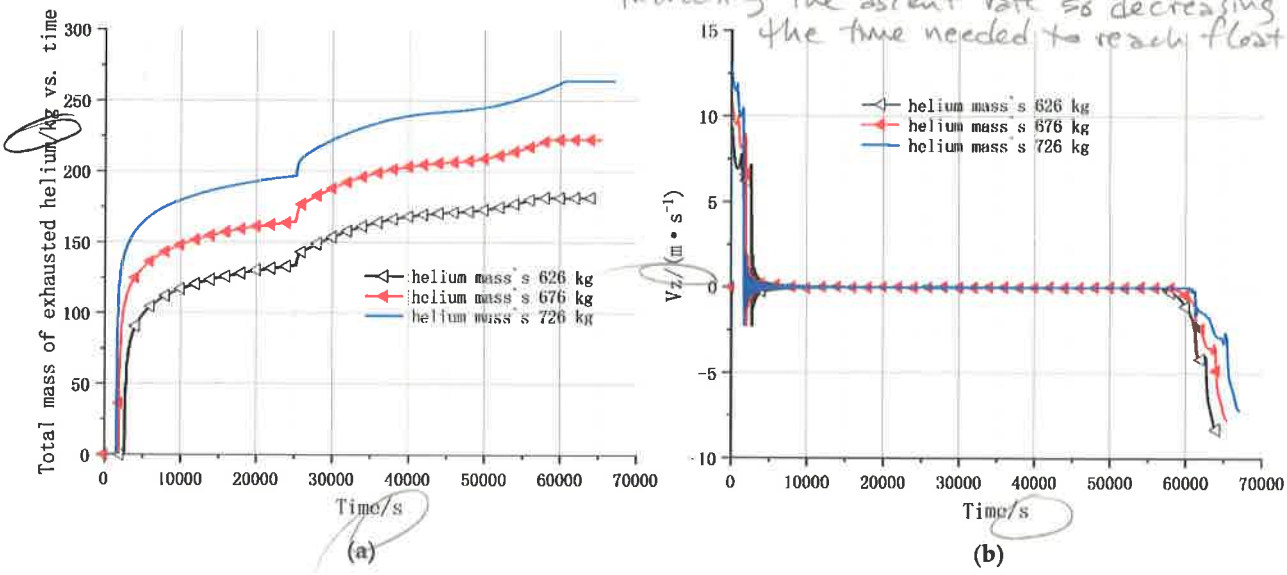
Figure 11. This figure shows the corresponding diagrams of different launch time. (a) shows the total mass of exhausted helium vs. time; (b) shows the change of vertical velocity; (c) shows the change of the altitude; (d) shows the trajectory prediction.

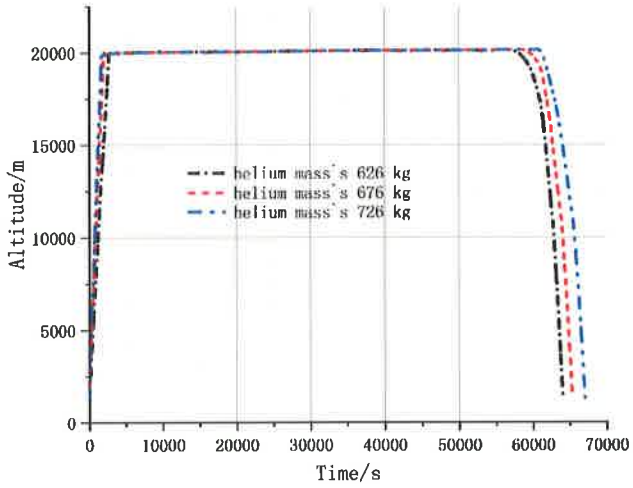
4.2.2. The Initial Helium Mass

The different initial helium mass including 626 kg, 676 kg and 726 kg are used to simulate the flight mission on 8 August 2019 (UTC+16). As shown in Fig. 12, the corresponding results are as follows:

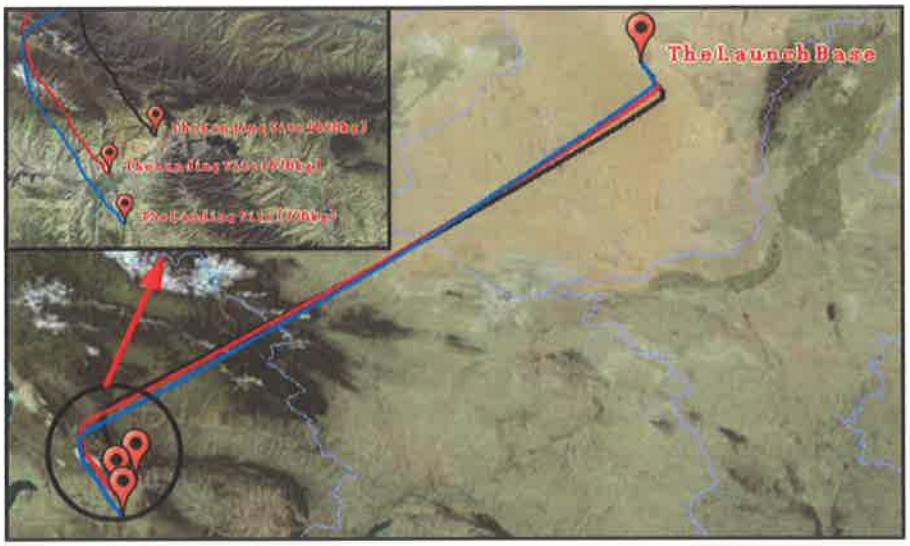
1. The more the initial mass of helium, the more the mass of helium is exhausted. However, the mass of helium inside the balloon is the same when landing.
2. The more initial mass of helium, the faster the balloon system ascends.
3. The initial mass of helium has no effect on the floating altitude and trajectory prediction.

Based on the above results, the initial mass of helium affects the flight performance during the ascent phase and has no effect on the floating and descending phase. The selection of the initial helium mass is determined by the requirements of the ascent velocity.





(c)



(d)

Figure 12. This figure shows the corresponding diagrams of different initial mass of helium. (a) shows the total mass of exhausted helium vs. time; (b) shows the change of vertical velocity; (c) shows the change of the altitude; (d) shows the trajectory prediction.

4.3. *Trajectory Prediction with Control Strategy*

The above simulation results show that the zero-pressure balloon flight system flying in a huge airspace makes it difficult to recover the balloon system even considering the launch time. What's more, the landing speed of the balloon system is destructive to safe recovery. Based on these considerations, the corresponding control strategy is employed to plan the trajectory.

In this study, the active exhaust model and the ballast model are used coordinately to control the trajectory. Furthermore, the control strategy also takes the floating time and the wind speed profile into consideration, which is helpful for the real flight. The control strategy are as follows.

Most of the balloon flight missions just needs to float at the designed altitude for several hours or less. According to the above results, it's obvious that the zero-pressure is in the automatic exhaust phase for this time period. Then the balloon system begins to

enforce the active exhaust procedure to accelerate transition to descend after finishing the floating mission. When the balloon system begins to descend, the vertical speed increases simultaneously. The Fig. 13 shows the wind speed profile which is measured on 8 August 2019. From the diagram, it illustrates that the horizontal wind speed is excessively large from altitude of 10 km to altitude of 15 km, causing excessive horizontal motion of the balloon system in the corresponding range of altitude. There is no doubt that it's reasonable to traverse this height layers ASAP. After the above procedures finished, the landing speed needs to be optimized by the ballast model to ensure safe landing.

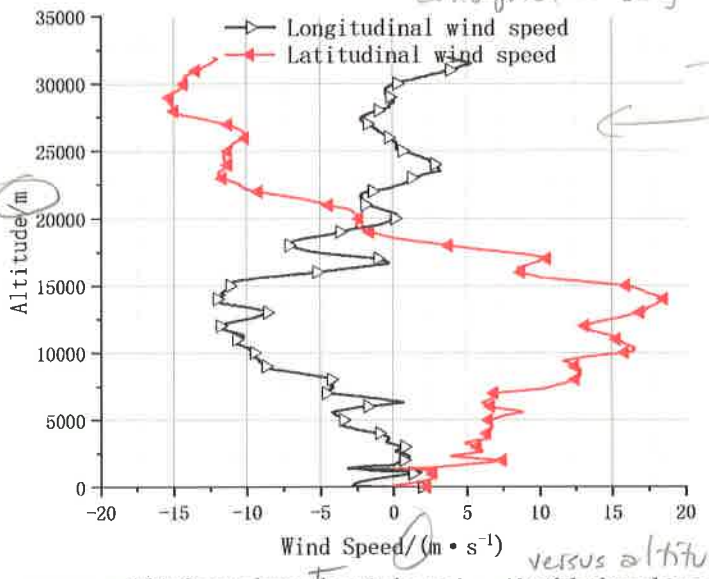


Figure 13. This figure shows the wind speed profile of the launching day.

Taking the floating mission time, horizontal motion and landing speed into consideration, the balloon flight system's trajectory simulation is as follows. The Table 2 shows the specification of the missions. Fig. 14 shows the change of vertical velocity. Fig. 15 shows the trajectory of different missions. The corresponding results are as follows:

1. With the control strategy applied, the flight time and lateral drift distance are greatly reduced. For Mission A, the straight-line distance is 63.17 km. For Mission C the straight-lien distance is 70.46 km. And for all the flight mission, the flight time is less than 3 hours. What's more, the landing velocity can reach 0.
2. The ballast flow rate mainly depends on the ballast throwed altitude for a certain flight mission.

Based on the above results, these help for the overall design of the balloon flight system and the flight mission can be finished within the limited airspace and lasts as little time as possible.

Table 2. Flight mission specifications.

Flight Mission	Floating time/min	Ballast Throwed Altitude/km	Ballast Flow Rate/(kg·s⁻¹)
Mission A	30	10	1.023
Mission B	30	8	1.671
Mission C	60	10	1.024

Mission D	60	8	1.672

* The launch time takes place at latitude 39° and longitude 105° on 8 August 2019 (UTC+16). And the initial helium mass is 626 kg.

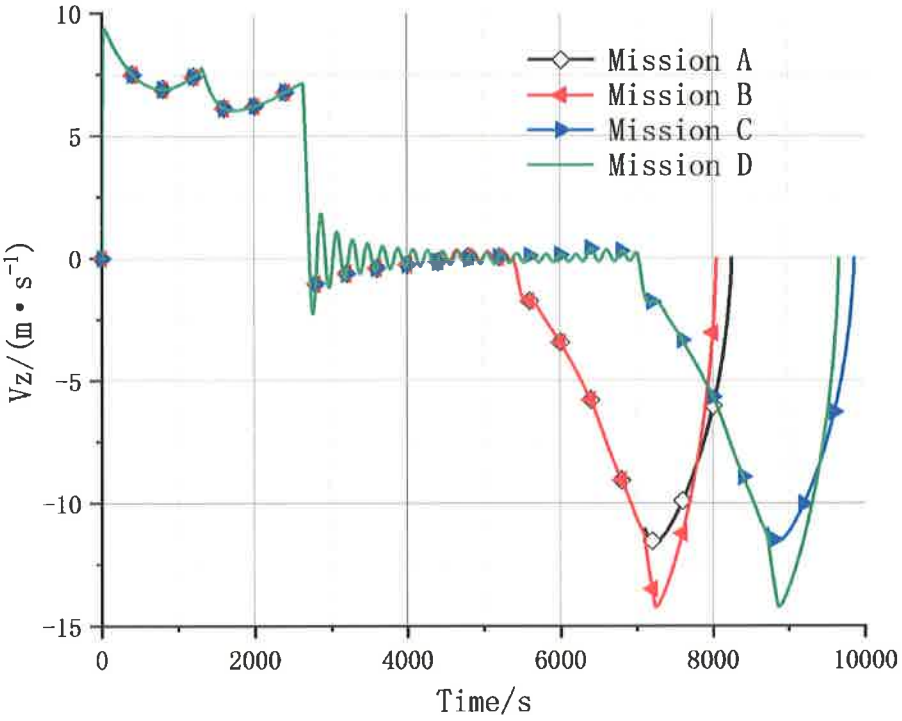


Figure 14. This figure shows the balloon system's change of vertical speed.

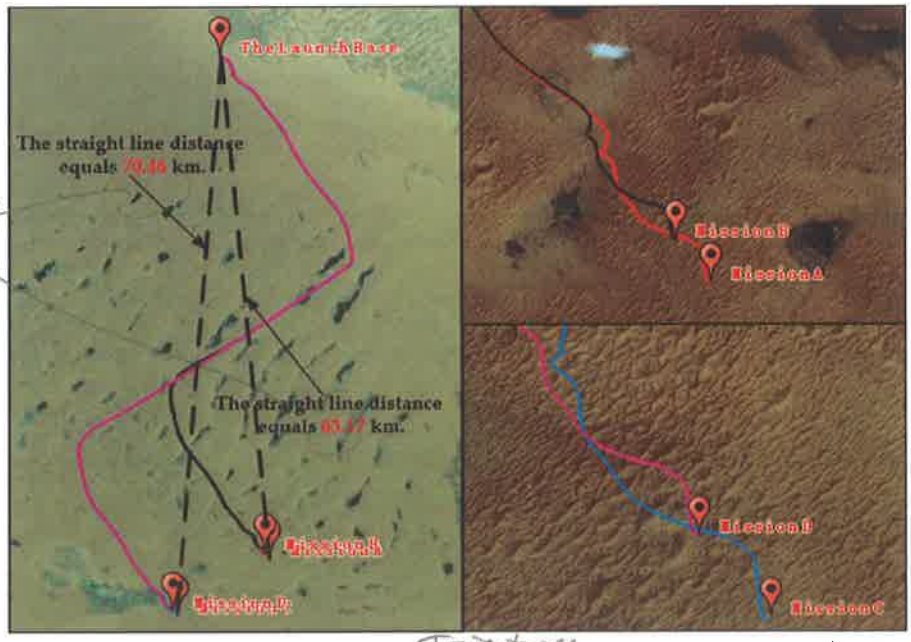


Figure 15. This figure shows the trajectory of different flight missions.

5. Conclusions

The high-altitude zero-pressure balloon flight system almost flies with the wind in the horizontal direction, so it's necessary to predict the trajectory in advance, preventing the balloon flight system from flying out the required airspace and avoiding the possible accidents. At the same time, most balloon flight system needs to fly within the limited airspace and realize rapid recovery of the balloon system, which contribute to save on flight mission costs.

In the present work, the high-altitude zero-pressure balloon flight system with no parachute is simulated to predict the trajectory, aiming to figure out clearly the balloon flight performance and improve rapid recovery. Through this work, the results can help the OEM of the balloon flight system improve its design and plan the flight missions. The conclusions of the work are as follows:

1. During the ascent phase, the vertical velocity takes on a W shape. By the time balloon flight system reaches the designed altitude, the vertical velocity decreases sharply to 0 and oscillates around 0 until it finally drops gradually to 0.
2. During the ascent phase, the phenomenon of supercooling occurs. While the phenomenon of superheating occurs at the phase of floating and descending phases. All of these help for the balloon structure design.
3. The launch time plays an important role in trajectory prediction. The results show that the earlier the launch time, the longer the flight time and the flight distance. However, the maximum flight time is less than 24 hours. The initial mass of helium almost has no effect on trajectory prediction.
4. Based on the real flight situation, the floating mission time, horizontal motion and landing speed are taken into consideration. The exhausted helium valve and throwing ballast device work coordinately to plan the trajectory to improve rapid recovery. The results show that the flight mission can be finished within the limited airspace and lasts as little time as possible. And the landing velocity can reach 0, which helps for the safe landing.
5. What's more, the ballast flow rate is determined by the ballast throwed altitude for a certain flight mission and determined experimentally by a throwing ballast device before the balloon flight mission.

Author Contributions: Conceptualization, Jiwei Tang, Shumin Pu; methodology, Shumin Pu and Jiwei Tang; software, Shumin Pu; validation, Jiwei Tang; formal analysis, Shumin Pu; investigation, Peixi Yu and Weicheng Xie; resources, Shumin Pu and Jiwei Tang; data curation, Yunfei Li; writing—original draft preparation, Peixi Yu and Binxing Hu; writing—review and editing, Shumin Pu and Jiwei Tang; supervision, Jiwei Tang; project administration, Jiwei Tang; funding acquisition, Jiwei Tang. All authors have read and agreed to the published version of the manuscript.

Funding: This work is supported by the National Natural Science Foundation of China under Grant No. 51906141 and Shanghai Sailing Program under Grant No. 19YF1421500.

Data Availability Statement: Not applicable.

Conflicts of Interest: The authors declare no conflict of interest.

References

1. Tang, Jiwei; Duan, Dengping, Xie Weicheng. "Shape Exploration and Multidisciplinary Optimization Method of Semirigid Nearing Space Airships." Journal of Aircraft 59, no. 4 (2021): 946-963.
2. Tang, Jiwei, Wang, Xiaoliang, Duan, Dengping, Xie, Weicheng. "Optimisation and analysis of efficiency for contra-rotating propellers for high-altitude airships." The Aeronautical Journal 123, no. 1263 (2019): 706-726.
3. Tang Jiwei, Xie Weicheng, Wang Xiaoliang and Chen Cheng. "Simulation and Analysis of Fluid-Solid-Thermal Unidirectional Coupling of Near-Space Airship." Aerospace 9, no. 439 (2022). https://doi.org/10.3390/aerospace9080439.
4. Yamada, Kazuhiko, Takashi Abe, Kojiro Suzuki, Naohiko Honma, Masashi Koyama, Yasunori Nagata, Daisuke Abe et al. "Deployment and flight test of inflatable membrane aeroshell using large scientific balloon." In 21st AIAA aerodynamic decelerator systems technology conference and seminar, p. 2579. 2011.

5. Jones, William Vernon. "Evolution of scientific ballooning and its impact on astrophysics research." Advances in Space Research 53, no. 10 (2014): 1405-1414.
6. Randolph, Thomas M., Robert Mullenax, Christopher Schwantes, Steven W. Sell, and Danny RJ Ball. "The first balloon flight of the Low Density Supersonic Decelerator technology demonstration mission." In 2015 IEEE Aerospace Conference, pp. 1-12. IEEE, 2015.
7. Qu, Zhengyu, Cuichun Li, Yong Hao, Feng Yan, and Yanchu Yang. "Project of high altitude balloon launched micro glider: Aircraft design, control and flight test." International Journal of Micro Air Vehicles 12 (2020): 1756829320979955.
8. Gemignani, Matteo, and Salvo Marcuccio. "Dynamic characterization of a high-altitude balloon during a flight campaign for the detection of ISM radio background in the stratosphere." Aerospace 8, no. 1 (2021): 21.
9. Farley, Rodger. "BalloonAscent: 3-D simulation tool for the ascent and float of high-altitude balloons." In AIAA 5th ATIO and16th Lighter-Than-Air Sys Tech. and Balloon Systems Conferences, p. 7412. 2005.
10. Dai, Qiumin, Xiande Fang, Xiaojian Li, and Lili Tian. "Performance simulation of high altitude scientific balloons." Advances in Space Research 49, no. 6 (2012): 1045-1052.
11. Sóbester, András, Helen Czerski, Niccolò Zapponi, and Ian Castro. "High-altitude gas balloon trajectory prediction: a Monte Carlo model." AIAA journal 52, no. 4 (2014): 832-842.
12. Zhang, Yi, and Dongxu Liu. "Influences of initial launch conditions on flight performance of high altitude balloon ascending process." Advances in Space Research 56, no. 4 (2015): 605-618.
13. Lee, Yongseon, and Kwanjung Yee. "Numerical prediction of scientific balloon trajectories while considering various uncertainties." Journal of Aircraft 54, no. 2 (2017): 768-782.
14. Saleh, Sherif, and Weiliang He. "Ascending performance analysis for high altitude zero pressure balloon." Advances in Space Research 59, no. 8 (2017): 2158-2172.
15. Atmosphere, US Standard. US standard atmosphere. National Oceanic and Atmospheric Administration, 1976.
16. Cathey H M. Advances in the thermal analysis of scientific balloons[R]. AIAA 1996-9605, 1996.
17. Cheng Chen, Wang Xiaoliang. Thermodynamic model of airship considering skin transmittance and its thermal characteristics[J]. Journal of Shanghai Jiaotong University,2021,55(07):868-877.
18. DAI Qiumin. Study on thermal environment and thermal characteristics of airships[D]. Nanjing: Nanjing University of Aeronautics and Astronautics, 2014.
19. Kreider, J. F. "Mathematical modeling of high altitude balloon performance." In 5th Aerodynamic Deceleration Systems Conference, p. 1385. 1975.
20. Rogers R. M. Applied Mathematics in Integrated Navigation Systems. American Institute of Aeronautics and Astronautics, Inc., 2000. ISBN 1-56347-397-6.
21. Sum of Sine Models. Available online: https://ww2.mathworks.cn/help/curvefit/sum-of-sine.html (accessed on 2 August 2022).
22. Robyr, J-L., Vincent Bourquin, Damien Goetschi, Nicolas Schroeter, and Richard Baltensperger. "Modeling the vertical motion of a zero pressure gas balloon." Journal of Aircraft 57, no. 5 (2020): 991-994.
23. Lv Mingyun, Wu Zichun. Thermodynamic model and numerical simulation of high altitude balloon ascending process [J]. Journal of Beijing University of Aeronautics and Astronautics, 2011,037(005):505-509. (in Chinese)
24. Farrell J. A. and Barth M. The Global Positioning System & Inertial Navigation. McGraw Hill, 1999. ISBN 0-07-022045-X.
25. Yajima, Nobuyuki, Naoki Izutsu, Takeshi Imamura, and Toyoo Abe. Scientific Ballooning: Technology and applications of exploration balloons floating in the stratosphere and the atmospheres of other planets . Vol. 112. Springer Science & Business Media, 2009.
26. Garde, Gabriel. "Comparison of two balloon flight simulation programs." InAIAA 5th ATIO and16th Lighter-Than-Air Sys Tech. and Balloon Systems Conferences, p. 7413. 2005.
27. Palumbo, R., "A Simulation Model for Trajectory Forecast, Performance Analysis and Aerospace Mission Planning with High Altitude Zero Pressure Balloons," Ph.D. Dissertation, University of Naples "Federico II," Naples, Italy, 2008.